22. G. P. Wakeham, D. D. Chung, K. A. Nelson, *Thermochim. Acta* **384**, 7 (2002).
23. P. R. Poulin, K. A. Nelson, in *Ultrafast Phenomena XIV*, T. Kobayashi, T. Okada, T. Kobayashi, K. A. Nelson, S. De Silvestri, Eds. (Springer-Verlag, Berlin, 2005), pp. 529–531.
24. I. Benjamin, U. Banin, S. Ruhman, *J. Chem. Phys.* **98**, 8337 (1993).
25. E. C. M. Chen, W. E. Wentworth, *J. Phys. Chem.* **89**, 4099 (1985).
26. D. W. Brenner, *Phys. Rev. B* **42**, 9458 (1990).
27. D. W. Brenner *et al.*, *J. Phys. Condens. Matter* **14**, 783 (2002).
28. Z. Bihary, M. Karavitis, V. A. Apkarian, *J. Chem. Phys.* **120**, 7576 (2004).
29. J. N. Sherwood, Ed., *The Plastically Crystalline State (Orientationally-Disordered Crystals)* (Wiley, New York, 1978).
30. We thank P. Mueller for assistance in recording x-ray diffraction spectra. This work was supported in part by grants from the Office of Naval Research (N00014-01-1-0802 and N00014-06-1-0459).

Supporting Online Material
www.sciencemag.org/cgi/content/full/1127826/DC1
Materials and Methods
Fig. S1
References

23 March 2006; accepted 17 August 2006
Published online 31 August 2006;
10.1126/science.1127826
Include this information when citing this paper.

Anomalous Increase in Carbon Capacitance at Pore Sizes Less Than 1 Nanometer

J. Chmiola,[1] G. Yushin,[1] Y. Gogotsi,[1]* C. Portet,[2]† P. Simon,[2] P. L. Taberna[2]

Carbon supercapacitors, which are energy storage devices that use ion adsorption on the surface of highly porous materials to store charge, have numerous advantages over other power-source technologies, but could realize further gains if their electrodes were properly optimized. Studying the effect of the pore size on capacitance could potentially improve performance by maximizing the electrode surface area accessible to electrolyte ions, but until recently, no studies had addressed the lower size limit of accessible pores. Using carbide-derived carbon, we generated pores with average sizes from 0.6 to 2.25 nanometer and studied double-layer capacitance in an organic electrolyte. The results challenge the long-held axiom that pores smaller than the size of solvated electrolyte ions are incapable of contributing to charge storage.

Supercapacitors, also called electrical double-layer capacitors (EDLCs), occupy a region between batteries and dielectric capacitors on the Ragone plot describing the relation between energy and power (*1*). They have been touted as a solution to the mismatch between the fast growth in power required by devices and the inability of batteries to efficiently discharge at high rates (*2*, *3*). This large capacity for high power discharge is directly related to the absence of charge-transfer resistances that are characteristic of battery Faradaic reactions and subsequently leads to better performance at low temperature. Improvements in the energy density may accelerate the advent of electrical and fuel-cell cars, as well as enable numerous industrial and consumer applications for supercapacitors (*4*). Improvements have been made in cell packaging and electrolytes (*5*, *6*), but a lack of substantial progress in carbon material design has limited energy density, effectively preventing wide-scale usage of supercapacitors.

Unlike batteries and fuel cells that harvest energy stored in chemical bonds, supercapacitors exploit the electrostatic separation between electrolyte ions and high–surface area electrodes, typically carbon (*1*). This results in capacitances of tens of Farads per gram of active material, unlike traditional dielectric capacitors that have capacitances typically measured in microfarads. Energy stored in supercapacitors is linearly proportional to the capacitance of its electrodes, making material optimization crucial.

The large capacitance, C, and hence energy storage potential, of supercapacitors arises due to the small (~1 nm) separation, d, between electrolyte ions and carbon and high (typically 500 to 2000 m^2/g) specific surface area (SSA) of carbon electrodes according to

$$C = \frac{\varepsilon A}{d} \quad (1)$$

where A is the electrode surface area accessible to electrolyte ions, and ε is the electrolyte dielectric constant. Because SSA is explicitly related to pore size, understanding its effect on specific capacitance is especially important and has been the subject of numerous studies over the past decade (*7*–*9*).

Traditional methods of producing porous carbon from either natural precursors such as coconut shell or synthetic precursors such as phenolic resin do not offer sufficient control over porosity (*10*). Mesoporous carbons synthesized by template techniques have produced controllable pores in the range of 2 to 4 nm (*11*). It is believed that pores substantially larger than the size of the electrolyte ion and its solvation shell are required for high capacitance. The use of carbon nanotubes (*12*) has provided a good model system with large pores and high conductivity, leading to impressive power densities but low energy density.

A less well-known class of porous carbons offers great potential for controlling pore size. Carbide-derived carbons (CDCs) are produced by high-temperature chlorination of carbides, whereby metals and metalloids are removed as chlorides, leaving behind nanoporous carbon with a 50 to 80% open pore volume (*13*). Atomic-level porosity control in CDC is achieved by exploiting the host carbide lattice as a template, permitting controlled layer-by-layer metal extraction by optimizing the chlorination parameters. CDCs have a narrow pore-size distribution with a mean value that is tunable with better than 0.05-nm accuracy in the range of ~0.5 to ~3 nm (*14*) and a SSA up to 2000 m^2/g (*15*), which make them attractive candidates for studying porosity in supercapacitor applications. The ease of pore tunability in CDC previously allowed experimental determination of the optimal pore size for hydrogen storage (*16*). Also, CDC has shown impressive specific capacitance when used as the active material in supercapacitors with many electrolyte systems (*17*–*20*). The use of CDC allows precise control over properties found in all carbon materials, allowing broad trends to be discovered that are applicable to other carbons. Previous work with titanium carbide–derived carbon (TiC-CDC) as the active material in supercapacitors with aqueous H_2SO_4 electrolyte (*18*) showed a correlation between the micropore size (pores <2 nm) and capacitance but did not explore pores smaller than 1 nm. This study focused on the small-pore effect by using CDC with pores tuned from 0.6 to 2.25 nm and an electrolyte consisting of a 1.5 M solution of tetraethylammonium tetrafluoroborate in acetonitrile.

TiC-CDC was synthesized by chlorination at 500° to 1000°C (*21*), and its bulk properties were characterized by Raman spectroscopy and transmission electron microscopy (TEM). Conductivity measurements were performed on compacted powders. Porosity was characterized by argon sorption at 77 K and confirmed with data from small-angle x-ray scattering (SAXS) (*22*) and CO_2 sorption at 300 K. The use of multiple techniques for porosity measurement ensures greater confidence in the results. Elec-

[1]Department of Materials Science and Engineering and A. J. Drexel Nanotechnology Institute, Drexel University, Philadelphia, PA 19104, USA. [2]Université Paul Sabatier, CIRIMAT, UMR CNRS 5085, 31062 Toulouse Cedex 4, France.

*To whom correspondence should be addressed. E-mail: gogotsi@drexel.edu

†Present address: Department of Materials Science and Engineering, Drexel University, Philadelphia, PA 19104, USA.

trochemical characterization on two- and three-electrode cells was performed with galvanostatic techniques for measuring capacitance and impedance spectroscopy to measure frequency response. No attempt was made to separate contributions from the positive and negative electrode to detect possible ion sieving because most of the pores were larger than the diameter of the largest unsolvated ion.

TiC-CDC microstructural and porosity development has previously been very well characterized (*18*, *20*), making it an ideal candidate for this study. To determine microstructural development, previous x-ray diffraction (XRD) results have shown that TiC is completely converted to CDC at synthesis temperatures >400°C, and no Bragg peak corresponding to graphite is visible even at a synthesis temperature of 1000°C (*21*). Similar to previous studies, Raman spectroscopy (Fig. 1A) showed a decreasing $R = I_D/I_G$ ratio, the ratio of graphite band (1582 cm^{-1}) intensity to disorder-induced band (~1350 cm^{-1}) intensity, with increasing synthesis temperature, indicating increasing ordering, but as seen previously in XRD, no large-scale graphitization. TEM micrographs (fig. S1, A to C) also showed gradual short-range ordering with rising synthesis temperature. The conductivity increased with synthesis temperature because of a reduction in the concentration of electron scattering defects (Fig. 1A). CDC had a higher conductivity compared to activated carbons from organic precursors with a similar porosity or surface area because it lacked oxygen or hydrogen in its carbon network (*13*).

Several techniques were used to determine the pore size and SSA of CDC. Nonlinear density functional theory (NLDFT) analysis of argon adsorption isotherms (fig. S2A) showed that the width of the pore-size distribution increased with synthesis temperature (fig. S2, B and C), and the average pore size shifted to larger values (Fig. 1B). The pore-size values obtained are in agreement with those obtained via CO_2 sorption at 300 K (fig. S3B) and SAXS analysis (*22*). The BET (Brunauer, Emmet, Teller) SSA showed a similar increase (Fig. 1B). SSA was also calculated by using NLDFT analysis, assuming slit pores, and was later used to corroborate trends revealed with the BET method (fig. S3A). Because the smallest pore size measured by Ar sorption was equal to the unsolvated BF_4^- electrolyte ion size, all the surface area available to the electrolyte ions for charge storage was accessible to Ar. Two advanced activated carbons used commercially in supercapacitors, referred to as NMAC (natural material precursor activated carbon) and SMAC (synthetic material precursor activated carbon), were also studied and served as a reference. They had average pore sizes of 1.45 and 1.2 nm and SSAs of 2015 and 2175 m^2/g, respectively. CDCs synthesized from B_4C and Ti_2AlC (*17*), which have pore sizes of 1.25 and 2.25 nm, respectively, and SSAs of 1850 and 1150 m^2/g, respectively, were also studied because their pore sizes are close to those of typical activated carbons. The results showed that CDC synthesized in the temperature range studied had a pore structure representative of a wide range of activated carbons, making it a good model system to study the effect of pore size on energy storage.

The electrochemical behavior of TiC-CDC is shown in Fig. 2. These results were repeated in experiments at both Drexel University and the University of Paul Sabatier with minimal deviation. The traditional understanding of how porosity affects specific capacitance and frequency response holds that pores larger than the size of the electrolyte ion plus its solvation shell are required for both minimizing the characteristic relaxation time constant, τ_0 (*23*) (the minimum time needed to discharge all the energy from the supercapacitor cell with an efficiency >50%), and maximizing its specific capacitance (*24*). Therefore, because conductivity, surface area, and average pore size all scaled with synthesis temperature, it was expected that CDC synthesized at 1000°C would exhibit the shortest τ_0 and the highest capacitance. Indeed, increasing the average pore size from 0.68 to 1.1 nm caused a slight decrease in τ_0 (Fig. 2A, inset), as expected. Even for the sample with the smallest pore size (500°C TiC-CDC), there was only a minimal decrease in specific capacitance when the current density was increased from 5 to 100 mA/cm^2 (Fig. 2B), which illustrates the minimal change in frequency-response behavior. NMAC and SMAC, which have pore sizes similar to those of TiC-CDC at 1000°C, had time constants similar to those of 800°C TiC-CDC, owing to the higher bulk conductivity of CDC. The opposite trend was found in the behavior of capacitance, however:

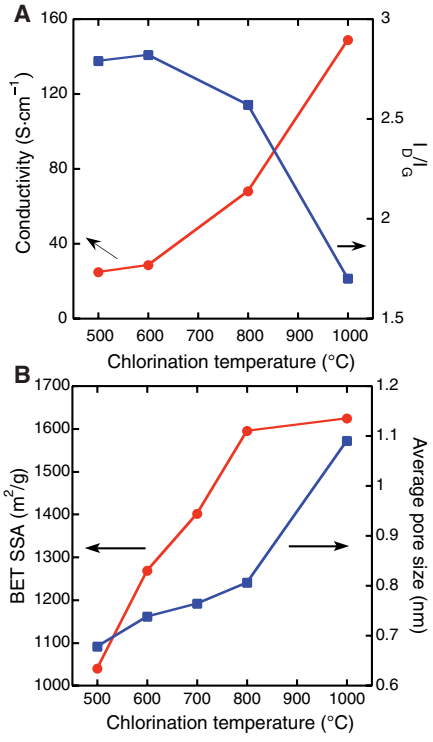

Fig. 1. Effect of synthesis temperature on structure and properties of CDC. The carbon structure (**A**) resolved by Raman spectroscopy showed a decreasing I_D/I_G ratio with increasing synthesis temperature, indicating increasing order. This increasing order was reflected in increasing conductivity with synthesis temperature. Porosity information resolved from gas sorption data shows (**B**) that both the SSA and average pore size increased with synthesis temperature. The calculated error between successive measurements of both pore size and SSA values are within only a few percent.

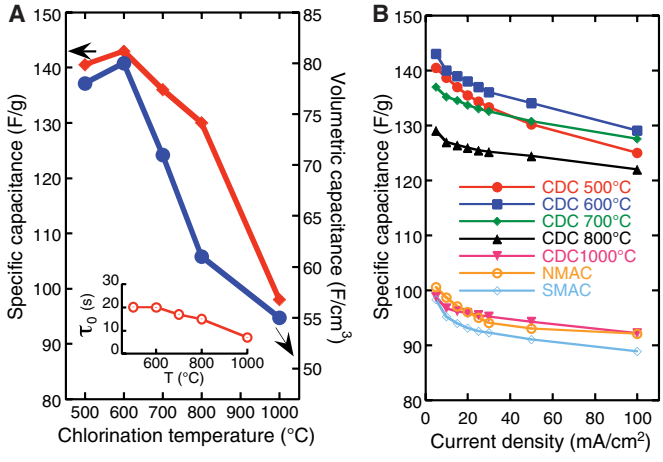

Fig. 2. Electrochemical behavior of TiC-CDC synthesized in the range of 500° to 1000°C. (**A**) Specific capacitance and volumetric capacitance both decreased with synthesis temperature. The maximum error reported in specific and volumetric capacitance was 2.5 and 6%, respectively. Maximum capacitance was at 600°C synthesis temperature. NAMAC and SMAC characteristics are 100 F/g, 35 F/cm^3 and 95 F/g, 45 F/cm^3, respectively, under the same conditions. The plot of characteristic time constant, τ_0, versus synthesis temperature (inset), showed slightly increasing frequency response with temperature. Comparison of TiC-CDC charge-discharge behavior with commercially available carbons (**B**) shows that by using rational design, a 50% improvement can be achieved. There was also very little capacitance fading at current densities up to 100 mA/cm^2, even for the 500°C sample.

Both the specific (gravimetric) and volumetric (capacitance per unit bulk volume of carbon) capacitances decreased with increasing synthesis temperature (Fig. 2A). With an increase in the chlorination temperature from 500° to 1000°C, the specific capacitance decreased by ~40%, from ~140 to ~100 F/g, although the SSA increased by ~60%, from 1000 to 1600 m^2/g. This decrease in capacitance in high–surface area carbons has been attributed to the development of surface area that was inaccessible to electrolyte ions due to the small size of the pores (*25*). In our study, however, the increasing surface area at elevated synthesis temperatures was exclusively the result of larger-diameter pores (Fig. 1B). Therefore, it cannot be explained by the traditional understanding.

When the specific capacitance was normalized by SSA, the effect of pore size, irrespective of surface area, could be ascertained (Fig. 3A). For TiC-CDC, increasing the pore size appeared to have a detrimental effect on the normalized capacitance. Although BET SSA is reported here because it is the most widely used technique and allows direct comparison with data from other studies, specific capacitance was also normalized by DFT SSA, which yielded the same trends (fig. S3A). These results are particularly interesting because the high capacitance of some carbons with pore sizes smaller than 1 nm has been noted before (*9*, *18*, *26*), but a model to explain this behavior has been lacking, and large pores are still considered optimal by most.

Figure 3A shows that there is a trend of decreasing normalized capacitance when the pore size is reduced to ~1 nm, based on data from this study and (*8*, *26*). TiC-CDC synthesized at 1000°C, B_4C-CDC, Ti_2AlC-CDC, NMAC, and SMAC all manifested this behavior, which demonstrated that this size effect was independent of the carbon material used. However, at a pore size below a critical value, as seen with TiC-CDC synthesized below 1000°C, the trend reversed and there was a sharp increase in capacitance with decreasing pore size. Two other carbons with small pores (*8*) follow the same trend.

In region I of Fig. 3A, when pores were substantially larger than twice the size of the solvated ions (Fig. 3B), there was a contribution to capacitance from compact layers of ions residing on both adjacent pore walls. Although the diffuse layer of charge that exists on a planar electrode, classically described by de Levie (*27*), was absent or diminished in size, the capacitance was largely unaffected because the compact layer encompasses much of the potential drop. Decreasing the pore size to less than twice the solvated ion size (Fig. 3C) reduced the normalized capacitance (Fig. 3A, region II) because compact ion layers from adjacent pore walls impinged and the surface area usable for double-layer formation was reduced. This would largely account for the decrease in specific capacitance with pore-size reduction for pore sizes greater than ~1 nm.

This trend reversed with a further decrease in the pore size to less than that of the solvated ion size (Fig. 3D, region III). Decreasing the pore size to a value approaching the crystallographic diameter of the ion led to a 100% increase in normalized capacitance. Dzubiella and Hansen showed that under a potential, there is substantial ion motion and diminished dielectric permittivity in pores less than the size of their solvation shells (*28*). The solvation shell becomes highly distorted as the ion is squeezed through the pore in much the same way a balloon distorts when squeezed through an opening smaller than its equilibrium size. The distortion of solvation shells in small pores of carbon nanostructures was also reported recently (*29*–*31*). Such distortion would allow closer approach of the ion center to the electrode surface, which by Eq. 1, leads to improved capacitance. When the capacitance data from Fig. 3 for pore sizes smaller than the size of the solvated ion (~1 nm) were plotted against the reciprocal of the pore size, a linear relation was obtained (fig. S6). This simplified model, which assumes planar pore surface and constant dielectric permittivity, has important implications. The effects of surface curvature and decreasing dielectric permittivity should decrease the capacitance, which showed the dominance of the 1/*d* term. Whereas templated carbons achieve improved specific capacitance by an increase in the pore size (Fig. 3A, region I, and 3B), resulting in low volumetric capacitance, our model suggests that using microporous carbons with pores smaller than 1 nm allows the volumetric capacitance to increase from 55 to 80 F/cm^3 (Fig. 2A).

The demonstration of charge storage in pores smaller than the size of solvated electrolyte ions will lead to enhanced understanding of ionic transport in porous media. These findings should also permit the design of application-specific supercapacitors: for longer discharge times where energy density is at a premium, such as in hybrid electric vehicles, extremely narrow pores should prove optimal, but for pulse power applications, increasing the pore size might be beneficial. Further tuning the carbon porosity and designing the carbon materials with a large volume of narrow but short pores may allow both energy and power characteristics to be improved.

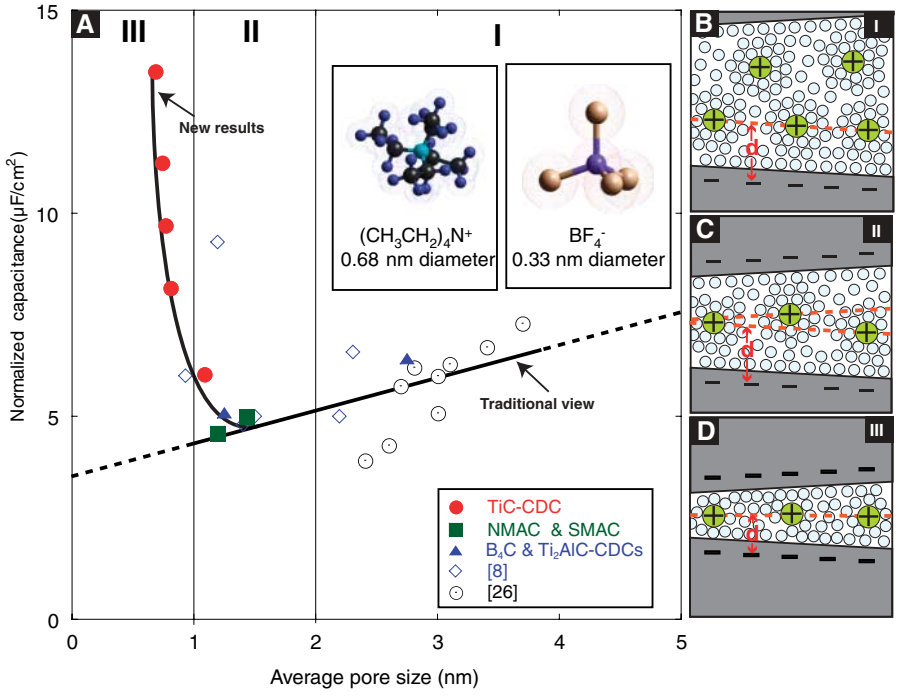

Fig. 3. (**A**) Plot of specific capacitance normalized by BET SSA for the carbons in this study and in two other studies with identical electrolytes. The normalized capacitance decreased with decreasing pore size until a critical value was reached, unlike the traditional view which assumed that capacitance continually decreased. It would be expected that as the pore size becomes large enough to accommodate diffuse charge layers, the capacitance would approach a constant value. (**B** to **D**) Drawings of solvated ions residing in pores with distance between adjacent pore walls (B) greater than 2 nm, (C) between 1 and 2 nm, and (D) less than 1 nm illustrate this behavior schematically.

References and Notes

1. B. E. Conway, *Electrochemical Capacitors: Scientific Fundamentals and Technological Applications* (Kluwer, Dordrecht, the Netherlands, 1999).
2. A. S. Arico, P. Bruce, B. Scrosati, J.-M. Tarascon, W. V. Schalkwijk, *Nat. Mater.* **4**, 366 (2005).

3. R. J. Brodd *et al.*, *J. Electrochem. Soc.* **151**, K1 (2004).
4. G. Woolfe, *Batteries Energy Storage Technol.* **3**, 107 (2005).
5. J. N. Barisci, G. G. Wallace, D. R. MacFarlane, R. H. Baughman, *Electrochem. Commun.* **6**, 22 (2004).
6. A. Rudge, J. Davey, I. Raistrick, S. Gottesfeld, J. P. Ferraris, *J. Power Sources* **47**, 89 (1994).
7. E. Frackowiak, F. Beguin, *Carbon* **39**, 937 (2001).
8. J. Gamby, P. L. Taberna, P. Simon, J. F. Fauvarque, M. Chesneau, *J. Power Sources* **101**, 109 (2001).
9. G. Salitra, A. Soffer, L. Eliad, Y. Cohen, D. Aurback, *J. Electrochem. Soc.* **147**, 2486 (2000).
10. F. Beguin, E. Frackowiak, in *Nanomaterials Handbook*, Y. Gogotsi, Ed. (CRC Press, Boca Raton, FL, 2006), pp. 713–737.
11. H. Zhou, S. Zhu, M. Hibino, I. Honma, *J. Power Sources* **122**, 219 (2003).
12. R. H. Baughman, A. A. Zakhidov, W. A. de Heer, *Science* **297**, 787 (2002).
13. G. Yushin, A. Nikitin, Y. Gogotsi, in *Nanomaterials Handbook*, Y. Gogotsi, Ed. (CRC Press, Boca Raton, FL, 2006), pp. 237–280.
14. Y. Gogotsi *et al.*, *Nat. Mater.* **2**, 591 (2003).
15. R. K. Dash, G. Yushin, Y. Gogotsi, *Micropor. Mesopor. Mat.* **86**, 50 (2005).
16. Y. Gogotsi *et al.*, *J. Am. Chem. Soc.* **127**, 16006 (2005).
17. J. Chmiola *et al.*, *Electrochem. Solid-State Lett.* **8**, A357 (2005).
18. J. Chmiola, G. Yushin, R. Dash, Y. Gogotsi, *J. Power Sources* **158**, 765 (2006).
19. A. Janes, L. Permann, M. Arulepp, E. Lust, *Electrochem. Commun.* **6**, 313 (2004).
20. P. Zetterstrom *et al.*, *J. Phys. Condens. Matter* **17**, 3509 (2005).
21. Materials and methods are available as supporting material on *Science* Online.
22. G. Laudisio *et al.*, *Langmuir*, in press.
23. P. L. Taberna, P. Simon, J. F. Fauvarque, *J. Electrochem. Soc.* **150**, A292 (2003).
24. M. Endo *et al.*, *J. Electrochem. Soc.* **148**, A910 (2001).
25. H. Shi, *Electrochim. Acta* **41**, 1633 (1996).
26. C. Vix-Guterl *et al.*, *Carbon* **43**, 1293 (2005).
27. R. de Levie, A. Vogt, *J. Electroanal. Chem.* **341**, 353 (1992).
28. J. Dzubiella, J. P. Hansen, *J. Chem. Phys.* **122**, 234706 (2005).
29. J. M. Di Leo, J. Maranon, *J. Mol. Struct.* **729**, 53 (2004).
30. M. Carrillo-Tripp, H. Saint-Martin, I. Ortega-Blake, *Phys. Rev. Lett.* **93**, 168104 (2004).
31. T. Ohkubo *et al.*, *J. Am. Chem. Soc.* **124**, 11860 (2002).
32. We thank R. K. Dash and D. Berrigan (Drexel University) for experimental help and J. E. Fischer (University of Pennsylvania) for numerous helpful discussions. J.C. was supported by an NSF IGERT Fellowship. C.P. was supported by Delegation Generale pour l'Armement (DGA) in France. This work was partially supported by Arkema, France. TEM was performed at the Regional Nanotechnology Facility at the University of Pennsylvania. Raman microspectroscopy was performed at the Materials Characterization Facility at Drexel University with the help of Z. Nikolov.

Supporting Online Material

www.sciencemag.org/cgi/content/full//1132195/DC1
Materials and Methods
Figs. S1 to S6
References

7 July 2006; accepted 10 August 2006
Published online 17 August 2006;
10.1126/science/1132195
Include this information when citing this paper.

Oxygen Isotope Variation in Stony-Iron Meteorites

R. C. Greenwood,[1]* I. A. Franchi,[1] A. Jambon,[2] J. A. Barrat,[3] T. H. Burbine[4]

Asteroidal material, delivered to Earth as meteorites, preserves a record of the earliest stages of planetary formation. High-precision oxygen isotope analyses for the two major groups of stony-iron meteorites (main-group pallasites and mesosiderites) demonstrate that each group is from a distinct asteroidal source. Mesosiderites are isotopically identical to the howardite-eucrite-diogenite clan and, like them, are probably derived from the asteroid 4 Vesta. Main-group pallasites represent intermixed core-mantle material from a single disrupted asteroid and have no known equivalents among the basaltic meteorites. The stony-iron meteorites demonstrate that intense asteroidal deformation accompanied planetary accretion in the early Solar System.

The terrestrial planets formed by the collision and merger of smaller bodies, over a period lasting up to 100 million years (My) after Solar System formation (*1*). The final stage of this process was marked by giant impacts that resulted in large-scale planetary melting (*2*). As a consequence of their protracted formation histories, and subsequent geological reprocessing, the initial stages of planetary accretion are not recorded by these larger bodies. In contrast, asteroids preserve a record of the earliest stages of planetary growth. Thus, W isotopic analysis of iron meteorites (*3*) and Mg isotope studies of basaltic meteorites (*4*) indicate that the earliest asteroids accreted within 1 My of Solar System formation and, due to the presence of live ^{26}Al, rapidly underwent near-total melting.

However, the usefulness of asteroidal material in understanding the earliest stages of planetary formation is hindered by the fragmentary nature of the meteorite record. As a result, we are unable to say how many asteroids are represented in our meteorite collections (*5*). Oxygen isotope analysis is one method that has proven useful in understanding the relationships between the various meteorite sample suites (*6*). The melting event that caused the early-formed asteroids to segregate into a metal-rich core and silicate-rich mantle and crust also homogenized their oxygen isotopes (*7*). The later evolution of these bodies would be by mass-dependent fractionation processes, so that samples derived from the same source asteroid define a single mass fractionation line (slope ≈ 0.52) on a three-isotope diagram (*6*, *8*). Meteorite samples from melted asteroids are collectively referred to as differentiated achondrites.

One limitation with this technique results from the small-scale oxygen isotope variation displayed by many groups of differentiated achondrites (*6*). Thus, main-group pallasites, mesosiderites, and the howardite-eucrite-diogenite suite (HEDs) (*9*) all plot within the same area on an oxygen three-isotope diagram (*6*) and could, in theory, have come from a single asteroid. However, mineralogical and textural evidence indicates that these groups formed in distinct settings, with the HEDs and mesosiderites coming from the outer crust of an asteroid, whereas the main-group pallasites formed deep within their parent body (*10*). Because reflectance spectra indicate that HEDs are from the relatively intact asteroid 4 Vesta (*11*), the main-group pallasites must come from a separate source (*10*). To address the problem of such overlapping oxygen isotope variation, we have undertaken a detailed study of the main-group pallasites and mesosiderites by laser-assisted fluorination (*12*). The high analytical precision of this technique enables the offset between parallel mass fractionation lines to be measured to within ±0.02‰ (*12*) and therefore has the potential to resolve the overlaps seen in the differentiated achondrites.

The results of oxygen isotope analyses (*13*) unambiguously resolve the mesosiderites from the main-group pallasites; thus, each group defines a distinct linear array on an oxygen isotope variation diagram (Fig. 1). The mean Δ^{17}O (*8*) value is –0.183 ± 0.018 (2σ) for the main-group pallasites and –0.245 ± 0.020 (2σ) for the mesosiderites (*13*).

The mean Δ^{17}O value for the mesosiderites is indistinguishable from the previously determined HED value of –0.238 ± 0.014 (*7*). Furthermore, if data from laser-assisted fluorination studies of the HEDs are combined (*7*, *14*), the range in δ^{18}O values for the mesosiderites and HEDs are virtually identical (Fig. 1). It has long been known that the silicate portion of the mesosiderites and the various lithologies of the HED suite show strong mineralogical and geochemical similarities (*10*).

[1]Planetary and Space Sciences Research Institute, Open University, Walton Hall, Milton Keynes, MK7 6AA UK. [2]Laboratoire Magmatologie et Géochimie Inorganique et Expérimentale, Université Pierre et Marie Curie, CNRS UMR 7047 case 110, 4 place Jussieu, 75252 Paris Cedex 05, France. [3]Université de Bretagne Occidentale–Universitaire Européen de la Mer, CNRS UMR 6538 (Domaines Océaniques), place Nicolas Copernic, F-29280 Plouzané Cedex, France. [4]Department of Astronomy, Mount Holyoke College, South Hadley, MA 01075, USA.

*To whom correspondence should be addressed. E-mail: r.c.greenwood@open.ac.uk

Anomalous Increase in Carbon Capacitance at Pore Sizes Less Than 1 Nanometer

J. Chmiola *et al.*

Science **313**, 1760 (2006);
DOI: 10.1126/science.1132195